ACS APPLIED MATERIALS & INTERFACES

RESEARCH ARTICLE

www.acsami.org

Solvothermal Synthesis of Crystalline Phase and Shape Controlled Sn^{4+}-Doped TiO_2 Nanocrystals: Effects of Reaction Solvent

Jia Liu, Yin Zhao,* Liyi Shi,* Shuai Yuan, Jianhui Fang, Zhuyi Wang, and Meihong Zhang

Research Center of Nanoscience and Nanotechnology, Shanghai University, 99 Shangda Road, Shanghai 200444, P R China. Fax & Tel: +86-21-66134852

Supporting Information

ABSTRACT: The Sn^{4+}-doped TiO_2 nanocrystals with controlled crystalline phase and morphology had been successfully prepared through easily adjusting the solvent system from the peroxo-metal-complex precursor by solvothermal method. The Sn^{4+}-doped TiO_2 nanocrystals were characterized by XRD, Raman, TEM, HRTEM, XPS, ICP-AES, BET, and UV−vis. The experimental results indicated that the Sn^{4+}-doped TiO_2 nanocrystals prepared in the pure water or predominant water system trend to form rodlike rutile, whereas the cubic-shaped anatase Sn^{4+}-doped TiO_2 nanocrystals can be obtained in the alcohol system. The growth mechanism and microstructure evolution of the Sn^{4+}-doped TiO_2 nanocrystals prepared in the different solvent systems are discussed. The liquid-phase photocatalytic degradation of phenol was used as a model reaction to test the photocatalytic activity of the synthesized materials. It was found that sample Sn^{4+}-doped TiO_2 prepared in 1-butanol showed the maximum photoactivity, which attributed to higher band gap, optimal crystalline phase and surface state modifications.

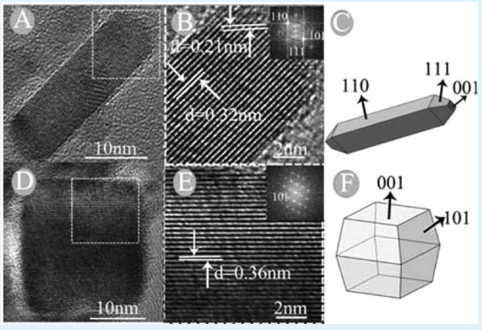

KEYWORDS: TiO_2, crystalline phase, morphology, solvothermal, photocatalytic activity

1. INTRODUCTION

TiO_2 nanocrystal has been increasingly focused because of its great potential applications in pigments, photochromic devices and gas sensors,[1−4] especially used as photocatalyst to decompose pollutions.[5,6] TiO_2 exists in three crystallographic forms in nature: anatase, rutile and brookite. Anatase is regarded as the most reactive phase due to the improved hole trapping resulted from steeper band bending.[7,8] And rutile not only is the most stable phase even in strong acidic or basic environments, but also has higher dielectric constant and better photo absorption property in visible light wavelength range (>400 nm).[9−13] In addition, many researchers have reported that morphology is also an important factor to the applications of TiO_2. Li et al. reported that changing the shape of nanocrystals can be provide more variable electronic states than changing the size of the system.[14] Gong et al. reported the anatase TiO_2 dominated by (001) surface is much more photocatalytic activity than that dominated by (101) surface.[15] Thus it is necessary to study the properly preparation of TiO_2 with controlled crystalline phase and morphology.

Many methods such as sol−gel method,[16] solvothermal process,[17] chemical vapor deposition,[18] and reverse microemulsion method[19] have been used for the synthesis of TiO_2. In these methods, sol−gel method is widely used to prepared nanosized TiO_2, however the as-synthesized precipitates in many cases are amorphous and subsequent heat treatment is necessary to induce crystallization. This step inevitably results in particle growth or destruction of the particle morphology.[20] Solvothermal synthesis, in which chemical reactions occur in aqueous or organic media under the self-produced pressure at relatively low temperature, is regarded as the most useful technique to synthesize nanocrystal TiO_2 because solvent behaviors much differently from that expected at the normal conditions.[21] For instance, Wang et al. successfully synthesized anatase TiO_2 with high crystallinity under 100 °C by solvothermal method.[22] Li et al. prepared monodisperse TiO_2 nanoparticles and nanorods by solvothermal method when using mixed NH_4HCO_3 and linoleic acid as reaction solvents.[23] In addition, it is found that the solvent plays an important role in controlling the crystalline phase and morphology of TiO_2. Liao et al. synthesized anatase TiO_2 nanocrystal colloid with controlled morphology through solvothermal reaction and found that ethanol is inclined to show more strongly adsorption to the (001) plane, which depressed the growth rate along the [001] direction and transformed the particle shape from "rodlike" to "rectangular".[17] Zhang et al. prepared high-performance fibrous TiO_2 photocatalysts with controlled crystalline phase by the solvothermal reaction and discussed the relationship between the dielectric constants of different solvents.[24]

Nowadays, several studies focus on the improvement of the photocatalytic activity of TiO_2 by metal ions doping.[25,26] However, little is known about the effects of different reaction solvent on the formation and properties of metal-ion-doped TiO_2

Received: January 19, 2011
Accepted: February 28, 2011
Published: February 28, 2011

dx.doi.org/10.1021/am2000642 | *ACS Appl. Mater. Interfaces* 2011, 3, 1261–1268

nanocrystals prepared by solvothermal method. It can be inferred that, for metal-ion-doped TiO_2 system, the different reaction solvents necessarily cause different effects on the dopant metal ions and Ti^{4+} ion in TiO_2 matrix owing to their different properties such as ionic radius, electronegativity etc. Thus, it is desired to research the location of dopant metal ions in the TiO_2 lattice, the microstructure, surface properties and optical properties of metal-ion-doped TiO_2 prepared in different reaction solvents, which can be provide a better understanding of growth mechanism and microstructure evolution of metal-ion-doped TiO_2 during different solvothermal synthesis process.

In our previous studies, we synthesized the Sn^{4+}-doped TiO_2 nanocrystal colloid from peroxo-metal complex solutions (PMC) by hydrothermal method.[27] In this research, the Sn^{4+}-doped TiO_2 nanocrystals with constant dopant Sn^{4+} ions content were prepared by different reaction solvents from peroxo-metal-complex precursor through the solvothermal route. The effects of different solvent on the essential structural properties of the resultant Sn^{4+}-doped TiO_2 nanocrystals such as the crystalline phase formation and the morphology were systematically investigated. The growth mechanism of the Sn^{4+}-doped TiO_2 nanocrystals prepared in different solvent systems was discussed. The photocatalytic activities of the synthesized materials were tested by using the liquid-phase photocatalytic degradation of phenol as a model reaction.

2. EXPERIMENTAL SECTION

2.1. Materials. All chemicals were used as received without further purification. Titanium(IV) sulfate ($Ti(SO_4)_2$, CR) and tin(IV) chloride pentahydrate ($SnCl_4 \cdot 5H_2O$, CR) were provided from Shanghai Chemical Reagent Co., China. Aqueous ammonia solution (NH_4OH, 25%, AR), aqueous hydrogen peroxide solution (H_2O_2, 30%, AR), absolute ethanol (C_2H_5OH, AR), 1-butanol (1-C_4H_9OH, AR), and phenol (AR) were purchased from Sinopharm Chemical Reagent Co. Ltd. Deionized water was used for solution preparation.

2.2. Preparation of the Sn^{4+}-Doped TiO_2 Nanocrystals. For the synthesis of Sn^{4+}-doped TiO_2 materials, titanium(IV) sulfate ($Ti(SO_4)_2$, CR) and tin(IV) chloride pentahydrate ($SnCl_4 \cdot 5H_2O$, CR) were used as precursors. It is required stoichiometric proportions of 9:1 of these two precursors have been dissolved in deionized water under vigorous stirring in room temperature and keeping the total cation-concentration at $[Me^+]_{total}$ = 0.2 M. Three molar ammonia solution was slowly added, adjusting the pH value to 8.0, which produced a white precipitate in the solution immediately. After aging for 12 h, the resulting suspension was filtered and washed. A purified white precipitate was then obtained. The obtained cake was ultrasonically dispersed in 125 mL of reaction solvents for 0.5 h. Under continuous magnetic stirring, 5.0 mL of H_2O_2 (30 wt %) was added dropwise to the suspension. The mixture was refluxed at 95 °C for 4 h. Finally, the solvothermal precursor was transferred to a Teflon autoclave and then held at 180 °C for 15 h. After the solvothermal crystallization, the prepared Sn^{4+}-doped TiO_2 nanocrystals were thus obtained. In present study, TSW, TSW_4E_1, TSW_1E_4, TSE, and TSB correspond to the samples prepared in pure water, 4:1 water/ethanol volume ratio, 1:4 water/ethanol volume ratio, ethanol, and 1-butanol, respectively.

2.3. Characterization. The Sn^{4+}-doped TiO_2 powders were prepared through rotatory evaporation at 50 °C for the following testing. The XRD analysis was performed using a Rigaku D/MAX-2550 X-ray diffractometer at room temperature, operating at 40 kV and 200 mA, using Cu Kα radiation (λ) 0.15418 nm. The average particle size is calculated by the Scherrer equation from the width of the most intense reflections: (101) for anatase and (110) for rutile. The weight fraction of anatase phase (denoted as x) also estimated from the XRD data by means of the following equation

$$x = 0.884I_A/(0.884I_A + I_R) \quad (1)$$

where I_A and I_R the integrated areas of the (101) peak of anatase and the (110) peak of rutile, respectively.[29] The Raman spectra were recorded on an in Via$^+$ Reflex spectrometer equipped with an optical microscope at room temperature, For excitation, the 514.5 nm line from an Ar^+ ion laser (Spectra Physics) was focused, with an analyzing spot of about 1 μm, on the sample under the microscope. The power of the incident beam on the sample was 1mW. The time of acquisition was varied according to the intensity of the Raman scattering. The TEM images were recorded on a JEOL TEM-200 CX microscope at an acceleration voltage of 200 kV. The particle size was estimated by the measurement of at least 100 particles in the TEM images. The HRTEM images were obtained using a JEM-2010F microscope (JEOL, Tokyo, Japan) at an acceleration voltage of 200 kV. The surface area of as-prepared samples was determined using a nitrogen adsorption apparatus (model 3H-2000III, China). Elemental analysis was carried out by inductively coupled plasma atomic emission spectroscopy (ICP-AES) at Optima 7300DV. X-ray photoelectron spectroscopy (XPS) spectra were recorded by a PHI 5000C ESCA spectrometer using Mg Kα radiation ($h\nu$ = 1253.6 eV). The pressure of the analyzer chamber was maintained at 5×10^{-8} Pa. The shift of the binding energy due to relative surface charging was corrected using the C 1s level at 284.6 eV as an internal standard. The experimental spectra were resolved into Lorentzian−Gaussian components after subtraction of a linear background, using a nonlinear least-squares fitting route. The quantitative analysis of the sample was performed using the route software of the XPS instrument with appropriate sensitivity factors. Diffuse reflectance spectra (DRS) were obtained for the dry-pressed disk samples using a Scan UV−vis−NIR spectrophotometer (Varian, Cary 500) equipped with an integrating sphere assembly, using $BaSO_4$ as a reference sample.

2.4. Photocatalytic Degradation of Phenol. The photocatalytic activities of the Sn^{4+}-doped TiO_2 nanocrystals were evaluated by photocatalytic degradation of phenol under UV light illumination. 0.06 g

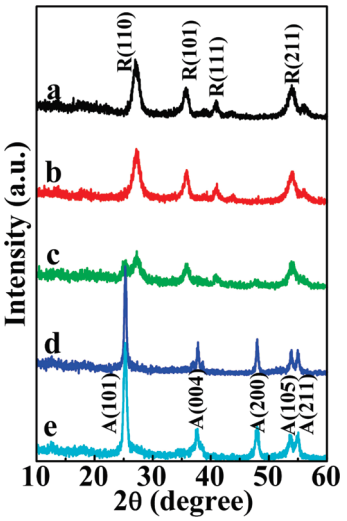

Figure 1. XRD patterns of the Sn^{4+}-doped TiO_2 nanocrystals: (a) TSW (the Sn^{4+}-doped TiO_2 nanocrystals prepared in pure water), (b) TSW_4E_1 (the Sn^{4+}-doped TiO_2 nanocrystals prepared in 4:1 water/ethanol volume ratio mixed solvent), (c) TSW_1E_4 (the Sn^{4+}-doped TiO_2 nanocrystals prepared in 1:4 water/ethanol volume ratio mixed solvent), (d) TSE (the Sn^{4+}-doped TiO_2 nanocrystals prepared in ethanol), and (e) TSB (the Sn^{4+}-doped TiO_2 nanocrystals prepared in 1-butanol). A, anatase; R, rutile.

Table 1. Characteristics of the Sn^{4+}-Doped TiO_2 Nanocrystals

	$Ti_{1-x}Sn_xO_2$		XRD measurements				
sample[a]	calculate x	obtained x (ICP)[b]	phase detected	crystallite size (nm)	particle size (nm) from TEM	S_{BET} (m^2/g)	band gap (E_g)
TSW	0.10	0.100	rutile	7.0 ± 0.3	7.4	152.7 ± 0.7	3.1
TSW_4E_1	0.10	0.099	rutile	5.9 ± 0.3	8.2	129.9 ± 1.5	3.0
TSW_1E_4	0.10	0.100	anatase(26.6%)	7.6 ± 0.7	8.1	132.9 ± 0.9	3.1
			rutile	6.0 ± 0.6			
TSE	0.10	0.099	anatase	21.9 ± 0.7	22.7	93.3 ± 0.7	3.1
TSB	0.10	0.095	anatase	14.4 ± 0.6	16.7	89.2 ± 0.9	3.3

[a] TSW, TSW_4E_1, TSW_1E_4, TSE, and TSB correspond to the Sn^{4+}-doped TiO_2 nanocrystals prepared in pure water, 4:1 water/ethanol volume ratio, 1:4 water/ethanol volume ratio, ethanol, and 1-butanol, respectively. [b] the obtained amounts of Sn in the final products from ICP-AES.

of such catalyst was suspended in 60 mL phenol aqueous solution (10 mg/L) using a 120 mL quartz tube and a magnetic stirrer for better stirring. The black light lamps (GE, F8T5/BLB) were used as an illuminating source symmetrically placed around reactor and the irradiation intensity was 0.55 mW/cm^2. The catalysts were agitated for 30 min in the phenol solution without light to attain the equilibrium adsorption on the catalyst surface. During the photoreaction process, the mixed solution was irradiated by UV lamps with constant magnetic stirring. The phenol concentration of the solution was measured every 30 min after removing sample powders. The remaining solution was withdrawn for subsequent analysis with a UV−vis spectrophotometer (UV-2501 PC spectrometer). The efficiency of degradation in every photoreaction process was calculated from formula as follows

$$\text{phenol degradation } (\%) = (C_0 - C)/C_0 \times 100\% \qquad (2)$$

in which C_0 and C are the original phenol concentration after the adsorption/desorption reached equilibrium and residual phenol concentration after reaction.

3. RESULTS AND DISCUSSION

Figure 1 shows the X-ray diffraction (XRD) patterns of the Sn^{4+}-doped TiO_2 samples prepared in different reaction solvents. From Figure 1, it can be seen that TSW and TSW_4E_1 exhibit single rutile phase. With decreasing H_2O/ethanol volume ratio, a mixture of anatase and rutile crystalline form with an obvious predominance of the rutile phase is observed in sample TSW_1E_4. For samples TSE and TSB, anatase appears as the single phase. Briefly, with decreasing H_2O/ethanol volume ratio, the crystalline form of the Sn^{4+}-doped TiO_2 change from rutile to anatase. Moreover, there is not any diffraction peak corresponding to SnO_2 in patterns of all samples.[28] The average crystalline size of all as-prepared samples was calculated by Scherrer formula and collected in Table 1. The rutile crystalline sizes decrease from 7.0 to 5.9 nm with the decreasing H_2O/ethanol volume ratio from sample TSW to TSW_4E_1. In the case of coexistence of anatase and rutile phase sample (TSW_1E_4), an interesting result is that anatase crystal is a little bigger than the rutile crystal. According to the previous report, a critical particle size should be required the crystalline phase transformation from anatase to rutile, thus the rutile size should be bigger than anatase one in the coexistence of anatase and rutile phase TiO_2.[29] However, the different result is obtained in our study, which indicates the phase transformation occurs in a different mechanism. In the case of anatase form, the crystalline size of sample TSE is 21.9 nm, which is larger than that of sample TSB (14.4 nm). The change in crystalline size can be explained as the interchange reaction between the peroxo-metal-complex precursor and the reaction solvent with longer carbon chain suppressing the growth rate.[30]

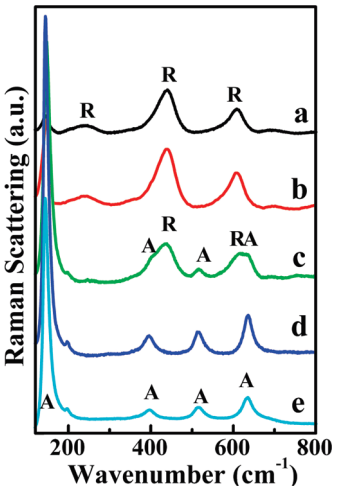

Figure 2. Raman spectra for the Sn^{4+}-doped TiO_2 nanocrystals: (a) TSW (the Sn^{4+}-doped TiO_2 nanocrystals prepared in pure water), (b) TSW_4E_1 (the Sn^{4+}-doped TiO_2 nanocrystals prepared in 4:1 water/ethanol volume ratio mixed solvent), (c) TSW_1E_4 (the Sn^{4+}-doped TiO_2 nanocrystals prepared in 1:4 water/ethanol volume ratio mixed solvent), (d) TSE (the Sn^{4+}-doped TiO_2 nanocrystals prepared in ethanol), and (e) TSB (the Sn^{4+}-doped TiO_2 nanocrystals prepared in 1-butanol). A, anatase; R, rutile.

The crystalline phase evolution of the Sn^{4+}-doped TiO_2 nanocrystals obtained in our work was also investigated by Raman spectroscopy and shown in Figure 2. In Figure 2, there are only rutile phase peaks at 146, 438, and 609 cm^{-1} in the samples TSW and TSW_4E_1, which is in agreement with the XRD results. With the increasing ethanol content in reaction solvent system (sample TSW_1E_4), there are three strong peaks at 143, 443, and 609 cm^{-1}, which are similar to those of rutile TiO_2,[16] three additional weak Raman peaks assigned to anatase phase of TiO_2 (398, 517, and 636 cm^{-1}) are also observed. The Raman result of the sample TSW_1E_4 indicates the anatase and rutile phase coexistence with predominance of the rutile. In the samples TSE and TSB, four bands at 146, 398, 514, and 638 cm^{-1} are observed, which assign to the characteristic peaks of anatase phases.[31] Moreover, the main Raman bands of SnO_2 crystalline form (776, 636, 574, and 490 cm^{-1}) are not detected, which indicates that tin does not exist as a separate crystalline oxide phase.[32] Therefore, the result of Raman spectroscopy in all samples further proves the XRD results.

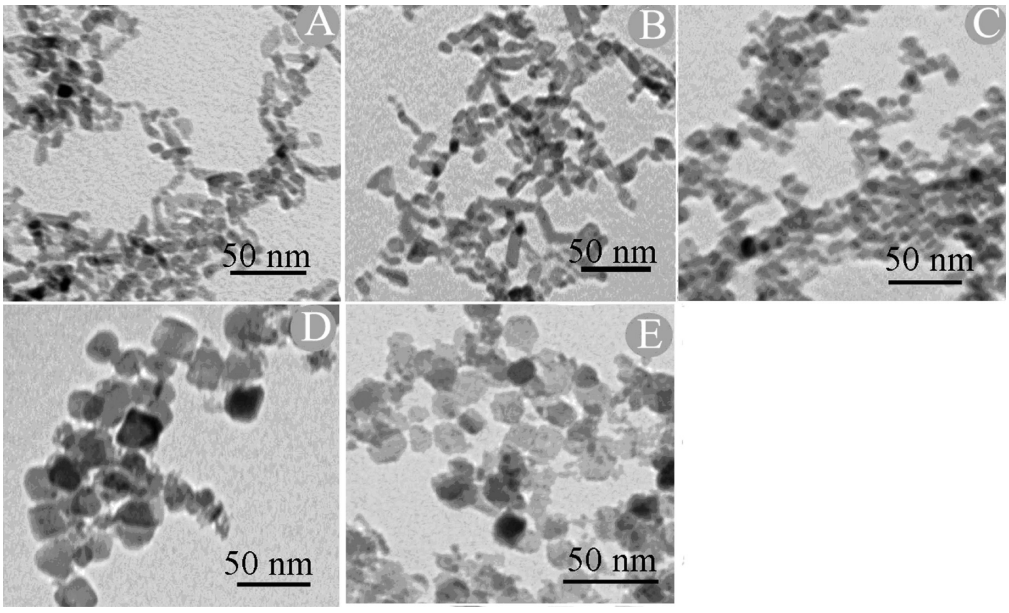

Figure 3. TEM images for the Sn^{4+}-doped TiO_2 nanocrystals: (A) TSW (the Sn^{4+}-doped TiO_2 nanocrystals prepared in pure water), (B) TSW_4E_1 (the Sn^{4+}-doped TiO_2 nanocrystals prepared in 4:1 water/ethanol volume ratio mixed solvent), (C) TSW_1E_4 (the Sn^{4+}-doped TiO_2 nanocrystals prepared in 1:4 water/ethanol volume ratio mixed solvent), (D) TSE (the Sn^{4+}-doped TiO_2 nanocrystals prepared in ethanol), and (E) TSB(the Sn^{4+}-doped TiO_2 nanocrystals prepared in 1-butanol).

The microstructural characterizations of the Sn^{4+}-doped TiO_2 nanocrystals were obtained by using TEM analysis (Figure 3 and Table 1). It can be observed that all the samples were well dispersed. The samples TSW, TSW_4E_1 and TSW_1E_4 show "rodlike" shape and have the similar particle size (Figure 3 and Table 1). However, the samples TSE and TSB exhibit "cubic-shape" (Figure 3D, E). The particle size of samples TSB is smaller than that of TSE. The samples with anatase phase show bigger particle sizes than above samples with rutile or coexistence of anatase and rutile phase. The Brunauer–Emmett–Teller (BET) surface areas of the Sn^{4+}-doped TiO_2 nanocrystal samples are shown in Table 1. The maximum surface area is observed for TSW sample with the value of 152.7 m^2/g. For the samples TSW_4E_1, TSW_1E_4 and TSE, it is obvious that the special surface areas decrease from 129.9 to 93.3 m^2/g with the increasing ethanol content in the mixed solvents. However, it is interesting to note that the surface area of TSB (89.2 m^2/g) is smaller than that of TSE (93.3 m^2/g) though the particle size of TSB is much smaller than that of TSE (Table 1). Comparing the special surface area S_{XRD} with the surface area using a nitrogen absorption S_{BET} (S_{XRD} is the special surface area valued by the formula of $S=6/d^*\rho$, where d is the particle size calculated by the Scherrer formula from XRD results and ρ is the density of anatase TiO_2), it is easily found that S_{BET}/S_{XRD} of sample TSE (S_{XRD} = 71.3 m^2/g, S_{BET}/S_{XRD} = 1.3) is higher than that of sample TSB (S_{XRD} = 108.4 m^2/g, S_{BET}/S_{XRD} = 0.822), which indicates sample TSE has more amorphous structure.[22]

To further study the surface composition and chemical states of the Sn^{4+}-doped TiO_2 nanocrystals, two representative samples TSW and TSB were characterized by XPS. Figure 4 shows the XPS spectra of Ti 2p (A), Sn 3d (B), and O1s (C and D) of samples TSW and TSB. It can be seen that XPS peak positions of Ti $2p_{3/2}$ and Ti $2p_{1/2}$ locate at approximately 458 and 464 eV, which indicates that Ti element mainly existed as the chemical state of Ti^{4+}.[33] XPS spectra of Sn 3d region are given in

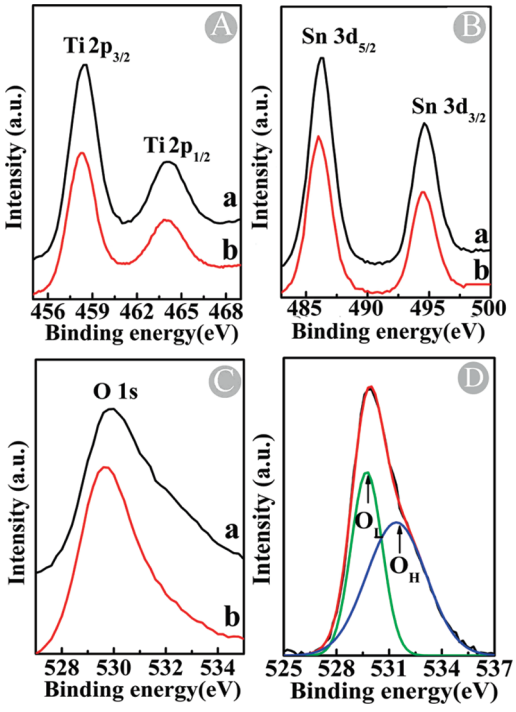

Figure 4. (A) Ti 2p, (B) Sn 3d, and (C) O1s XPS core level spectra of (a) TSW (the Sn^{4+}-doped TiO_2 nanocrystals prepared in pure water) and (b) TSB (the Sn^{4+}-doped TiO_2 nanocrystals prepared in 1-butanol); and (D) O 1s fitting results for sample TSB.

Figure 4B. The peak position corresponding to Sn $3d_{5/2}$ (Table 2) is located between that of Sn $3d_{5/2}$ in SnO_2 (486.5 eV) and Sn $3d_{5/2}$ in metallic Sn (485.0 eV), which should be assign to incorporated Sn^{4+} in the lattice of TiO_2.[34] From XPS spectra of O 1s core level of samples TSB and TSW in Figure 4C, they are

Table 2. Surface Analysis by XPS Spectra for the Sn^{4+}-Doped TiO_2 Nanocrystals

	binding energy (eV)						
sample[a]	Ti $2p_{3/2}$	Sn $3d_{5/2}$	O_L 1s(Ti−O)	O_H 1s(O−H)	$Ti_{1-x}Sn_xO_2$, x obtained from XPS	O_L (%)	O_H (%)
TSW	458.2	486.0	529.6	530.8	0.13	51.9	48.1
TSB	458.4	486.4	529.7	531.5	0.21	46.8	53.2

[a] TSW and TSB are corresponding to the Sn^{4+}-doped TiO_2 nanocrystals prepared in pure water and 1-butanol, respectively.

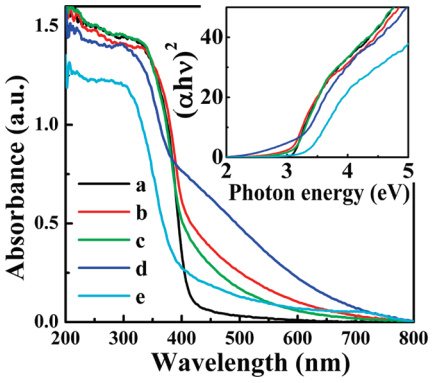

Figure 5. UV−vis diffuse reflectance spectra of the Sn^{4+}-doped TiO_2 nanocrystals: (a) TSW (the Sn^{4+}-doped TiO_2 nanocrystals prepared in pure water), (b) TSW_4E_1 (the Sn^{4+}-doped TiO_2 nanocrystals prepared in 4:1 water/ethanol volume ratio mixed solvent), (c) TSW_1E_4 (the Sn^{4+}-doped TiO_2 nanocrystals prepared in 1:4 water/ethanol volume ratio mixed solvent), (d) TSE (the Sn^{4+}-doped TiO_2 nanocrystals prepared in ethanol), and (e) TSB (the Sn^{4+}-doped TiO_2 nanocrystals prepared in 1-butanol). Inset shows the corresponding plot of $(\alpha h\nu)^2$ versus photon energy for the as-prepared samples.

asymmetric, indicating there are at least two kinds of chemical forms. After curve fitting, for sample TSB, one peak is at the binding energy of 529.7 eV corresponding to oxygen in TiO_2 lattice (O_L) and the other is 531.5 eV corresponding to oxygen in TiO_2 surface adsorption of H_2O (O_H) (Figure 4 and Table 2). The fitting results listed in Table 2 give the corresponding XPS data and atomic number ratio. As seen from Table 2, the amount of surface hydroxyl group is enhanced by transforming solvent system from water to 1-butanol.

Figure 5 shows the UV−vis diffuse reflectance spectra of the Sn^{4+}-doped TiO_2 samples. The optical band gap energy can be estimated by using the following equation for a semiconductor

$$\alpha = \frac{K(h\nu - E_g)^{n/2}}{h\nu} \quad (3)$$

where α is the absorption coefficient, K is a constant, E_g is the band gap, and n is equal to 1 for the direct transition. The band gap can be estimated from the plot of $(\alpha h\nu)^2$ versus photon energy ($h\nu$). The intercept of the tangent to the plot will give a good approximation of the band gap energy for this direct band gap material (shown in the inset of Figure 5).[35] The band gap energies of the Sn^{4+}-doped TiO_2 samples were calculated and listed in Table 1. From Figure 5, it could be seen that TSW_4E_1 (curve b) exhibits a slight red shift as compared to sample TSW (curve a), the band gap energy decrease from 3.10 to 3.00 eV, which might results from quantum size effects.[36] Rutile TSB exhibits a blue shift as compared to anatase TSW, and the band gap energy increase from 3.10 to 3.30 eV, which result from the effect of

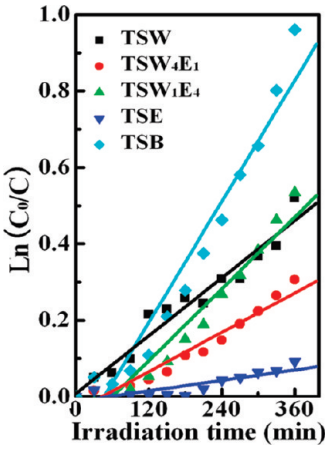

Figure 6. Linear transform $\ln(C_0/C) = kt$ of the kinetic curves of phenol disappearance. TSW, TSW_4E_1, TSW_1E_4, TSE, and TSB correspond to the Sn^{4+}-doped TiO_2 nanocrystals prepared in pure water, 4:1 water/ethanol volume ratio, 1:4 water/ethanol volume ratio, ethanol, and 1-butanol, respectively.

Table 3. Kinetic Values for the Phenol Photodecomposition and Photocatalytic Ability Results for the Sn^{4+}-Doped TiO_2 Nanocrystals

sample[a]	degradation of phenol (%)[b]	apparent rate constant k (h^{-1})	half-life $t_{1/2}$(h)
TSW	42.6 ± 1.0	0.00126	9.2
TSW_4E_1	26.4 ± 1.0	0.00157	7.4
TSW_1E_4	41.4 ± 1.0	0.000856	13.5
TSE	8.8 ± 1.0	0.000228	50.8
TSB	61.7 ± 1.0	0.00264	4.4

[a] TSW, TSW_4E_1, TSW_1E_4, TSE, and TSB correspond to the Sn^{4+}-doped TiO_2 nanocrystals prepared in pure water, 4:1 water/ethanol volume ratio, 1:4 water/ethanol volume ratio, ethanol, and 1-butanol, respectively. [b] the samples were irradiation under UV light for 6 h.

crystalline phase.[6,37] It is worthy noting that sample TSE displays an absorption edge corresponding to the visible light region. It might result from the undecomposed peroxo groups in sample TSE.[17]

Figure 6 shows that the photocatalytic degradation corresponds to a pseudo-first-order reaction. Pseudo-first-order kinetics was assumed to calculate the corresponding degradation rate constant (k):

$$\ln\left(\frac{C_o}{C}\right) = kt \quad (4)$$

where C_0 is the original phenol concentration after the adsorption/desorption reached equilibrium (mg L^{-1}), C is the

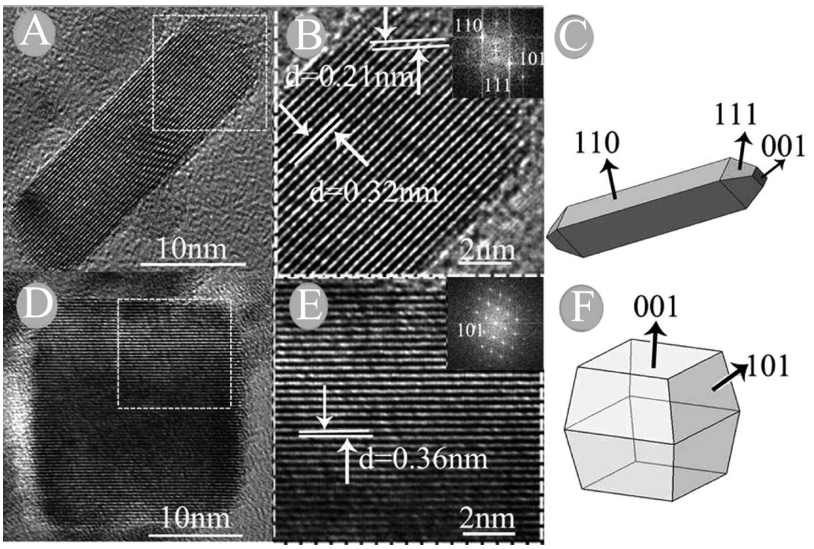

Figure 7. HRTEM of samples (A) TSW (the Sn^{4+}-doped TiO_2 nanocrystals prepared in pure water) and (D) TSB (the Sn^{4+}-doped TiO_2 nanocrystals prepared in 1-butanol); the selected area HRTEM enclosed by the dashed lines of samples (B) TSW and (E) TSB sketch the shape of (C) TSW and (F) TSB. The inset shows an FFT analysis of the anisotropic crystals.

concentration (mg L^{-1}) at a given time t (h) and k is the first-order degradation rate constant (h^{-1}). Half-life, $t_{1/2}$ (h), can be calculated from k by using the following equation

$$t_{1/2} = \frac{\ln 2}{k} \quad (5)$$

The photoactivity is calculated and reported as $t_{1/2}$ and the degradation rate of phenol in Table 3.

In the case of rutile samples, TSW shows a better performance than TSW_4E_1, suggesting a positive effect of higher surface area. However, the antase TSB with the lowest surface areas shows the maximum photocatalytic activity. This result attributes to not only crystalline phase, but also higher band gap and surface hydroxyl group affect the photocatalytic activity. Higher band gap indicates that higher redox potential. Surface hydroxyl group can play an important role in suppressing the recombination of the photogenerated electron−hole pairs.[38] However, anatase TSE exhibits the lowest efficiency, which may contribute to its poor crystallinity. Many researchers proved that the bicrystallline framework of anatase and rutile can effectively reduce the recombination of the photogenerated charge carrier to enhance the photocatalytic activity.[39,40] However, the coexistence of anatase and rutile phase sample TSW_1E_4 does not show higher photocatalytic activity than the rutile TSW or anatase TSB. It might result from that a large amount rutile phase in mixed-phase TSW_1E_4 can not make electrons transfer from rutile to anatase trapping sites, which makes the charge separate ineffectively and increases electron−hole recombination.[39] In summary, regarding to photocatalytic activity for degradation of phenol, TSB shows the maximum photoactivity due to higher band gap, optimal crystalline phase and surface state modifications.

4. MECHANISM ANALYSIS

Figure 7 shows the HRTEM and sketch shapes of two representational samples TSW and TSB. The HRTEM image of rutile TSW shows the rod-like shape (Figure 7A). The clear lattice fringes corresponded to a distance of 3.26 Å and 2.10 Å (Figure 7B), agree well with the distance of the (110) and (111) lattice planes of rutile TiO_2.[41] As Barnard et al. reported, the (110) surface of rutile has lower surface energy (average surface energy of 0.37 J/m^2) than the (001) surface (average surface energy of 0.57 J/m^2).[42] During the crystal growth, a fast growing plane with higher surface energy tends to disappear, leaving behind slower growing planes with lower surface energy. Thus, rutile nanocrystal TSW has grown into rod along the (001) direction and exhibited (110) facets (shown in Figure 7C).

For sample TSB, the lattice fringes shown in Figure 7E, corresponding to a distance of 3.66 Å, agree well with the distance of (101) lattice plane of anatase. The determination of sample TSB shape was performed by combining XRD and HRTEM. Three lines of the diffraction patterns for the crystal shape estimation were {101}, {004}, {200} corresponding to the displayed faces (101), (001) and (100) in anatase crystals.[43] The particle sizes in (101), (001) and (100) are 13.8, 15.4, and 13.6 nm, respectively. These three directions grow nearly equivalent in size, indicating the formation of cubic-shape particles. Lazzeri et al. used density functional theory to calculate the formation energies of the most common orientations of the anatase and found the energies for the relaxed surfaces (from highest to lowest) to rank as: (110) > (103) > (001) > (100) > (101).[44] Therefore, anatase (101) surface with relative lowest surface energy absolutely grows much slower than other directions. Many reporters maintain that the anatase TiO_2 trends to grow into (001) direction to display the "rod-like" shape.[17,44] However, samples TSB and TSE display cubic shape. Hengerer et al. reported that the adsorptions of methanol on (001) surface of TiO_2 is much stronger than that on (101) surface.[45] In addition, Yang et al. reported that the higher density of 5-fold Ti on (001) surfaces may adhere to 2-propanol because 2-propanol tends to heterolytically dissociate to form an alkoxy group bound to coordinatively unsaturated Ti^{4+} cations on the (001) surfaces, which retards the growth of anatase TiO_2 along the (001) direction.[36] 1-Butanol and ethanol have similar negative charges on the oxygen comparing to methanol and 2-propanol, which results in the similar activities of the alkoxy group bound to

coordinatively unsaturated Ti^{4+} cations on the (001) surfaces. Therefore, the growth of anatase TSB and TSE along the (001) direction is depressed.

In this research, the average compositions obtained from ICP-AES (Table 1) in all as-prepared Sn^{4+}-doped TiO_2 samples are in perfect accordance with those theoretical calculated data. The results indicate the synthesis of the Sn^{4+}-doped TiO_2 nanocrystals from peroxo-metal precursor by solvothermal method under the low temperature is available. In our previous work, we discussed the growth stages of Sn^{4+}-doped TiO_2 nanocrystals during the hydrothermal treatment.[27] Briefly, H_2O_2 first reacted with metal ions and then peroxo-metal complex precursor formed. After heated, the $[M(OH)_4(OH_2)_2]^0$ (M:Ti or Sn) growing units are formed. If the dopant Sn^{4+} ions content is high, the more $[Sn(OH)_4(OH_2)_2]^0$ basic structures trend to form, subsequently induce the rutile phase formation.[46] The sample TSW indeed reveals the rutile phase. However, anatase phase appears and becomes dominant with decreasing H_2O/ethanol volume ratio in reaction solvents (samples TSW_1E_4, TSB and TSE). It can be inferred that the different reaction solvents necessarily cause different effect on the dopant Sn^{4+} ions and Ti^{4+} in the TiO_2 matrix, which maybe induce different growth mechanism and microstructure evolution. The detailed explain list as follow. The electronegativity of Sn^{4+} (1.8) is remarkably greater than that of Ti^{4+} (1.5), so the charge on the six-coordinated surface tin atom of $[Sn(OH)_4(OH_2)_2]^0$ is significantly lower than the charge on the corresponding titanium atom of $[Ti(OH)_4(OH_2)_2]^0$.[47,48] Hence, the covalent bond between tin atoms and terminal oxygens will be enhanced with reducing charge, which reduces the negative charge of terminal oxygens on $[Sn(OH)_4(OH_2)_2]^0$ surface and labilizes the protons on the terminal oxygens.[48] The dehydrolysis between the labilited protons on $[Sn(OH)_4(OH_2)_2]^0$ surface and reaction solvents more prefer than corresponding $[Ti(OH)_4(OH_2)_2]^0$. In the alcohol or the predominant alcohol reaction system, the interaction between the $[Sn(OH)_4(OH_2)_2]^0$ and reaction solvents inevitably restrains the formation of rutile nuclei due to the steric effects of long alkyl chain. Thus, pure anatase Sn^{4+}-doped TiO_2 can be obtained using ethanol or 1-butanol as reaction media.

To confirm the assumption above, the crystallinity of pure SnO_2 prepared in water, mixed water/ethanol solvent, ethanol and 1-butanol are compared by XRD (see the Support Information). It can be seen that the crystallinity of SnO_2 prepared in mixed water/alcohol or alcohol solvent is relatively poor compared with the SnO_2 prepared in water. The proposal can also be confirmed by XPS and ICP-AES (Table 2) analysis. Generally, XPS analysis reflects the surface composition condition of as-prepared sample, while ICP-AES analysis could give the average composition condition. The deviation between XPS and ICP-AES dates of Sn^{4+} content can be calculated from the following formulation: Δ= (Sn^{4+} content obtained from XPS-Sn^{4+} content obtained from ICP-AES)/Sn^{4+} content obtained from ICP-AES. For sample TSB, ΔTSB (ΔTSB = (0.21−0.095)/0.095 =1.2, Tables 1 and 2) is much larger than that of sample TSE (ΔTSE = (0.13−0.10)/0.10 = 0.3, Tables 1 and 2), which indicates most of Sn^{4+} ions reside on the surface of TiO_2 particles in sample TSB. Therefore, for sample TSB, dopant Sn^{4+} is difficult to form a nucleus and induces the formation of rutile form. The results in this research provide a good confirmation that reaction solvents cause different effects on the dopant Sn^{4+} ions and Ti^{4+} ion in TiO_2 matrix, which lead to the different reactivity between the octahedral $[M(OH)_4(OH_2)_2]^0$ (M = Ti or Sn) units and solvents, therefore determine formation of crystalline phase even in the same of dopant Sn^{4+} ions content.

5. CONCLUSION

The Sn^{4+}-doped TiO_2 nanocrystals with controlled crystalline phase and morphology have been successfully synthesized through easily adjusting the reaction solvent system from the peroxo-metal-complex precursor by solvothermal method. The major effects of reaction solvent are: (i) with decreasing H_2O/alcohol ratio in reaction solvent, the crystalline form of the Sn^{4+}-doped TiO_2 with the same of Sn^{4+} doping content change from rutile to anatase; (ii) the change of crystalline form caused by the different reactivity between the octahedral $[M(OH)_4(OH_2)_2]^0$ (M = Ti or Sn) units and reaction solvents; (iii) the transformation from the "rod-like" to the "cubic-like" with the changes of water/alcohol ratio in reaction solvent due to the different adsorptions on crystal face by different solvents; (iv) the optical properties and surface hydroxyl group of the Sn^{4+}-doped TiO_2 nanocrystals change with the different reaction solvents. Regarding to the activity for the photocatalytic degradation of phenol, the Sn^{4+}-doped TiO_2 prepared in 1-butanol shows the maximum photoactivity because of higher band gap, optimal crystalline phase and surface state modifications.

■ ASSOCIATED CONTENT

Supporting Information. XRD patterns of the SnO_2 nanocrystals prepared in (a) H_2O, (b) 4:1 H_2O/ethanol volume ratio, (c) 1:4 H_2O/ethanol volume ratio, (d) ethanol, and (e) 1-butanol (PDF). This material is available free of charge via the Internet at http://pubs.acs.org.

■ AUTHOR INFORMATION

Corresponding Author

*E-mail: zhaoyin@shu.edu.cn (Y.Z.); shiliyi@shu.edu.cn (LY.S.).

■ ACKNOWLEDGMENT

The authors acknowledge the supports of the National Natural Science Foundation of China (Grant 21001072), Shanghai Leading Academic Discipline Project (S30107), International cooperation fund of Shanghai Science and Technology Committee (09520709500, 09520715400), The Research & Innovation Projects of Shanghai Education Commission (11YZ22).

■ REFERENCES

(1) Yuan, S.; Zhou, L.; Wu, B.; Yu, B. *J. Phys. Chem. B* **2006**, *110*, 388–394.

(2) James, R. J..; Andrei, G.; Laurence, M. P.; Patrik, S.; Alison, B. W. *J. Am. Chem. Soc.* **2008**, *130*, 13364–13372.

(3) Liu, G. H.; Zhu, Y. F.; Zhang, X. R.; Xu, B. Q. *Anal. Chem.* **2002**, *74*, 6279–6284.

(4) Vaidyanathan, S.; Zheng, Ni.; Seebauer, E. G.; Masel, R. I. *Ind. Eng. Chem. Res.* **2006**, *45*, 3815–3820.

(5) Yuan, S.; Sheng, Q. R.; Zhang, J. L.; Yamashita, H.; He, D. *Microporous Mesoporous Mater.* **2008**, *110*, 501–507.

(6) Linsebigler, A. L.; Lu, G. Q.; Yaters, T. J. *Chem. Rev.* **1995**, *95*, 735–758.

(7) Sumita, T.; Yamaki, T.; Yamamoto, S.; Miyashita, A. *Appl. Surf. Sci.* **2002**, *200*, 21–26.

(8) Riegel, G.; Bolton, J. R. *J. Phys. Chem.* **1995**, *99*, 4215–4224.

(9) Takagi, M. H.; Fujishiro, Y.; Awano, M. J. *Mater. Sci.* **2001**, *36*, 949–955.
(10) Ovenstone, J. *Mater. Sci.* **2001**, *36*, 1325–1329.
(11) Yang, K.; Zhu, J. M.; Zhu, J. J.; Huang, S. S.; Zhu, X. H.; Ma, G. B. *Mater. Lett.* **2003**, *57*, 4639–4642.
(12) Yang, S. F.; Liu, Y. H.; Guo, Y. P.; Zhao, J. Z.; Xu, H. F.; Wang, Z. C. *Mater. Chem. Phys.* **2002**, *77*, 501–506.
(13) Wu, M.; Lin, G.; Chen, D.; Wang, G.; He, D.; Feng, S.; Xu, R. *Chem. Mater.* **2002**, *14*, 1974–1980.
(14) Li, J.; Wang, L. W. *Nano Lett.* **2003**, *3*, 1357–1363.
(15) Gong, X. Q.; Selloni, A. *J. Phys. Chem. B.* **2005**, *109*, 19560–19562.
(16) Oliveira, M. M.; Schnitzler, D. C.; Zarbin, A. J. G. *Chem. Mater.* **2003**, *15*, 1903–1909.
(17) Liao, J. H.; Shi, L. Y.; Yuan, S.; Zhao, Y.; Fang, J. H. *J. Phys. Chem. C.* **2009**, *113*, 18778–18783.
(18) Cao, Y.; Yang, W.; Zhang, W.; Liu, G.; Yue, P. *New. J. Chem.* **2004**, *28*, 218–222.
(19) Fresno, F.; Tudela, D.; Coronado, J. M.; Soria, J. *Catal. Today* **2009**, *143*, 230–236.
(20) Niederberger, M.; Garnweitner, G.; Pinna, N.; Neri, G. *Prog. Solid. State. Chem.* **2005**, *33*, 59–70.
(21) Supphasrirongjaroen, P.; Kongsuebchart, W.; Panpranot, J.; Mekasuwandumrong, O.; Satayaprasert, C.; Praserthdam, P. *Ind. Eng. Chem. Res.* **2008**, *47*, 693–697.
(22) Wang, C.; Deng, Z.; Zhang, G. H.; Fan, S. S.; Li, Y. D. *Powder Technol.* **2002**, *125*, 39–44.
(23) Li, X. L.; Peng, Q.; Yi, J. X.; Wang, X.; Li, Y. D. *Chem.—Eur. J.* **2006**, *12*, 2383–2391.
(24) Zhang, P. L.; Yin, S.; Petrykin, V.; Kakihana, M.; Sato, T. *J. Mol. Catal. A: Chem.* **2009**, *309*, 50–56.
(25) Choi, W.; Termin, A.; Hoffmann, M. R. *J. Phys. Chem. B.* **1994**, *98*, 13669–13679.
(26) Bouras, P.; Stathatos, E.; Lianos, P. *Appl. Catal. B: Environ.* **2007**, *73*, 51–59.
(27) Zhao, Y.; Liu, J.; Shi, L. Y.; Yuan, S.; Fang, J. H.; Wang, Z. Y.; Zhang, M. H. *Appl. Catal. B: Environ.* **2010**, *100*, 68–76.
(28) Bouaine, A.; Brihi, N; Schmerber, G; Ulhaq-Bouillet, C; Colis, S.; Dinia, A. *J. Phys. Chem. C* **2007**, *111*, 2924–2928.
(29) Overstone, J.; Yanagisawa, K. *Chem. Mater.* **1999**, *11*, 2770–2774.
(30) H.Sakai, H.; Kawahara, M.; Shimazaki, M. Abe. *Langmuir* **1998**, *14*, 2208–2212.
(31) Zheng, R. Y.; Lin, L.; Xie, J. L.; Zhu, Y. X.; Xie, Y. C. *J. Phys. Chem. C* **2008**, *112*, 15502–15509.
(32) Leonardy, A.; Hung, W. Z; Tsai, D. S.; Chou, C. C.; Huang, Y. S. *Cryst. Growth Des.* **2009**, *9*, 3958–3963.
(33) Sanjines, R.; Tang, H.; Berger, H.; Gozzo, F.; Margaritondo, G. *J. Appl. Phys.* **1994**, *75*, 2945–1952.
(34) Xin, B.; Jin, L.; Ren, Z.; Wang, B.; Fu, H. *J. Phys. Chem. B* **2005**, *109*, 2805–2809.
(35) Zhao, Y.; Li, C. Z.; Liu, X. L.; Gu, F.; Du, H. L.; Jiang, H. B.; Shao, W.; Zhang, L.; He, Y. *Mater. Lett.* **2007**, *61*, 79–83.
(36) Liu, J. J.; Qin, W.; Zuo, S.; Yu, Y. C.; Hao, Z. P. J. *Hazard. Mater.* **2009**, *163*, 273–278.
(37) Koelsch, M.; Cassaignon, S.; Guillemoles, J. F.; Jolovet, J. P. *Thin Solid Film.* **2002**, *403*, 312–319.
(38) Chen, S.; Chen, L.; Gao, S.; Cao, G. *Mater. Chem. Phys.* **2006**, *98*, 116–120.
(39) Hurum, D. C.; Agrios, A. G.; Gray, K. A. *J. Phys. Chem. B.* **2003**, *107*, 4545–4549.
(40) Shi, L.; Weng, D. J. *Eviron. Sci.* **2008**, *20*, 1263–1267.
(41) TiO_2 (rutile), JCPDF card no. 21-1276.
(42) Barnard, A. S.; Zapol, P. *Phys. Rev.B.* **2004**, *70*, 235403–1−13.
(43) Durupthy, O.; Bill, J.; Aldinger, F. *Cryst. Growth Des.* **2007**, *7*, 2696–2704.
(44) Lazzeri, M.; Vittadini, A.; Selloni, A. *Phys. Rev.B.* **2001**, *63*, 155409–1−9.
(45) Hengerer, R.; Bolliger, B.; Erbudak, M.; Gratzel, M. *Surf. Sci.* **2000**, *460*, 162–169.
(46) Kumar, K. P.; Fray, D. J.; Nair, J.; Mizukamic, F.; Okubo, T. *Scr. Mater.* **2007**, *57*, 771–774.
(47) Rosenqvist, J.; Machesky, M. L.; Vlcek, L.; Cumming, P. T.; Wesolowski, D. J. *Langmuir* **2009**, *12*, 10852–10862.
(48) Sayilkan, H. *Appl. Catal., A* **2007**, *319*, 230–236.